Materials Science Forum Vols. 558-559 (2007) pp. 949-954
online at http://www.scientific.net

Online available since 2007/10/15

Faceting of Σ3 Grain boundaries in Al

S.G. Protasova[a], O.A. Kogtenkova[b] and B. Straumal[c]

Institute of Solid State Physics, Russian Academy of Sciences, 142432 Chernogolovka, Russia

[a]sveta@issp.ac.ru, [b] koolga@issp.ac.ru, [c]straumal@issp.ac.ru

Keywords: Grain boundary faceting, Al, twins, phase transitions

Abstract. The temperature dependence of the energy of various facets of twin GBs has been measured. For the investigation of GB faceting the Al bicrystals of 99.999% wt. purity were grown by the modified Bridgman technique. One grain in these bicrystals is semi-surrounded by another one. Bicrystals were coated with a layer of Sn–Al alloy and annealed at various temperatures. Contact angles at the junction of a GB and two solid/liquid interfaces have been measured. The ratios of GB energy to solid/liquid interface energy have been calculated. Using these data, the Wulff-Herring plots and GB phase diagrams were constructed. Three different crystallographic facets were observed for the coincidence GB. Two of them are stable at all studied temperatures, the third one becomes metastable below ~ 800K. In GBs with $\Delta\theta = 3°$ only one facet (symmetric twin GB) is stable.

Introduction

Faceting and roughening of grain boundaries (GBs) can drastically influence their properties and, thus, the properties of a polycrystal as a whole. In particular, GB faceting correlates with the phenomenon of abnormal grain growth in alumina [1], stainless steel [2], silver [3] and nickel-based superalloys [4]. It has been shown first for the free surfaces of a crystal, that each facet can become instable at certain roughening temperature T_R [5]. Above T_R the free energy for the formation of an elementary step at a surface becomes zero, and a facet becomes microscopically rough and macroscopically curved. The orientation of free surface facets is governed by a crystal lattice. In case of GBs the coincidence site lattice (CSL) plays the role similar to that of the crystal lattice for free surfaces. Namely, GB facets are usually parallel to the most densely packed CSL planes. New facets with lower and lower density of coincidence sites appear with decreasing temperature [6]. Moreover, the twin Σ=3 GB in a metal with low stacking fault energy (Cu) remains completely faceted up to the melting temperature [6]. The goal of this work is the direct measurement of twin GB energy in Al in dependence on GB inclination ϕ, temperature T and misorientation $\Delta\theta$. These data will reveal the difference in GB faceting behavior between fcc metals with low (Cu) and high (Al) stacking fault energy.

Experimental

For the investigation of GB faceting two Al (99.999 wt.% purity) bicrystals with a semi-island grain were grown using the modified Bridgman technique. Grain *2* in this bicrystal is semi-surrounded by grain *1* forming the Σ3 <110> tilt grain boundary (Fig. 1). One bicrystal has an exact coincidence tilt grain boundary Σ3 <110>. Second bicrystal has a GB with a misorientation deviated on $\Delta\theta = 3°$ degrees from Σ3 <110>. 5 mm thick platelets were cut from the grown bicrystals normal to the growth axis [7, 8]. The bicrystalline samples were coated with a layer of Sn–Al alloy and annealed in Ar gas atmosphere at pressure of 2×10^{-4} Pa and temperatures 723, 773, 823 and 873 K (0.77, 0.83, 0.88 and 0.94 of Al melting temperature T_m, respectively) during 2 hours. Then the samples were mechanically ground, polished and etched in a 50% HNO_3+47% HCl+3%HF solution. The contact angle α for various GB inclination angles ϕ, and geometry of facets was recorded in bright and dark field in the light microscope and measured (Fig. 1). The ratio of GB energy σ_{GB} to

solid/liquid interface energy σ_{SL} was calculated using the values of measured contact angle α: $\sigma_{GB} = 2\sigma_{SL} \cos(\alpha/2)$. The electron back-scattering diffraction (EBSD) method was used to determine the individual grain orientations in the Al bicrystals and the grain boundary shape in the as-grown bicrystals [7, 8]. In the samples under the investigation the misorientation deviation from coincidence tilt GB Σ3 <110> was less then 1° along the GB. It was significant that there were no triple junctions in the corners of the semi-surrounded grain, where the facets intersect.

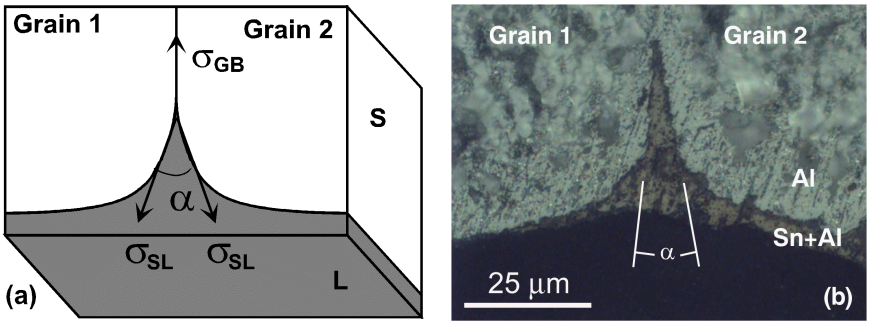

Fig. 1. Scheme (a) and micrograph (b) of the equilibrium contact between the grain boundary in the solid phase S and the liquid phase L (incomplete wetting).

Results and discussion

In Fig. 2 section of Σ3 CSL normal to <110> axis is shown. The closely packed CSL planes are shown together with the respective planes for the lattices *1* and *2* forming CSL. Exact Σ3 GB was fully faceted. In the exact Σ3 GBs three different facets were observed, namely symmetric Σ3 twin boundaries $\{111\}_1/\{111\}_2$ [or $(100)_{\Sigma3CSL}$] facets, the facet with angle of 82° with the symmetric twin boundary and the $\{100\}_1/\{122\}_2$ [or $(110)_{\Sigma3CSL}$] facets [8]. The $(110)_{\Sigma3CSL}$ facet has an angle of 56° with $(100)_{\Sigma3CSL}$ facet. The deviated Σ3 GB possess only one flat facet, namely symmetric Σ3 twins $\{111\}_1/\{111\}_2$ or $(100)_{\Sigma3CSL}$. Otherwhere the deviated Σ3 GB is curved [7].

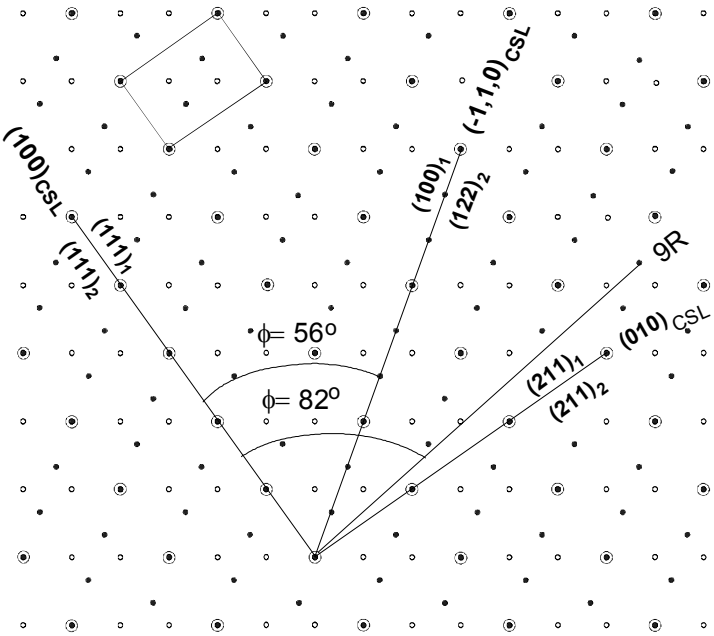

Fig. 2. Section of Σ3 CSL perpendicular to the {110} tilt axis with CSL unit cell and positions of $(100)_{\Sigma3CSL}$ and $(010)_{\Sigma3CSL}$ facets. Angle ϕ denotes an inclination of a GB.

In Fig. 3 the Wulff-Herring plots are shown for both Σ3 GBs at various temperatures. Wulff-Herring plots were constructed on the basis of σ_{GB}/σ_{SL} ratios measured using contact angle α. Thus, the method of an equilibrium contact with a liquid phase permitted us to construct the Wulff-Herring plots in a broad temperature interval. In our previous works the method of thermal groove has been used [6]. It permits to construct the Wulff-Herring plots only very close to T_m. In Fig. 3 the temperature dependence of ratio σ_{GB}/σ_{SL} for three different facets is shown. The energy of symmetric Σ3 twin $\{111\}_1/\{111\}_2$ [or $(100)_{\Sigma3CSL}$] facet is sufficiently low and does not change much during annealing at various temperatures. These facets are very stable and observed both in the exact Σ3 and deviated GBs. Similar situation is observed in Cu: the energy of $\{111\}_1/\{111\}_2$ or $(100)_{\Sigma3CSL}$ facet in Cu is very low and this facet is very stable [6].

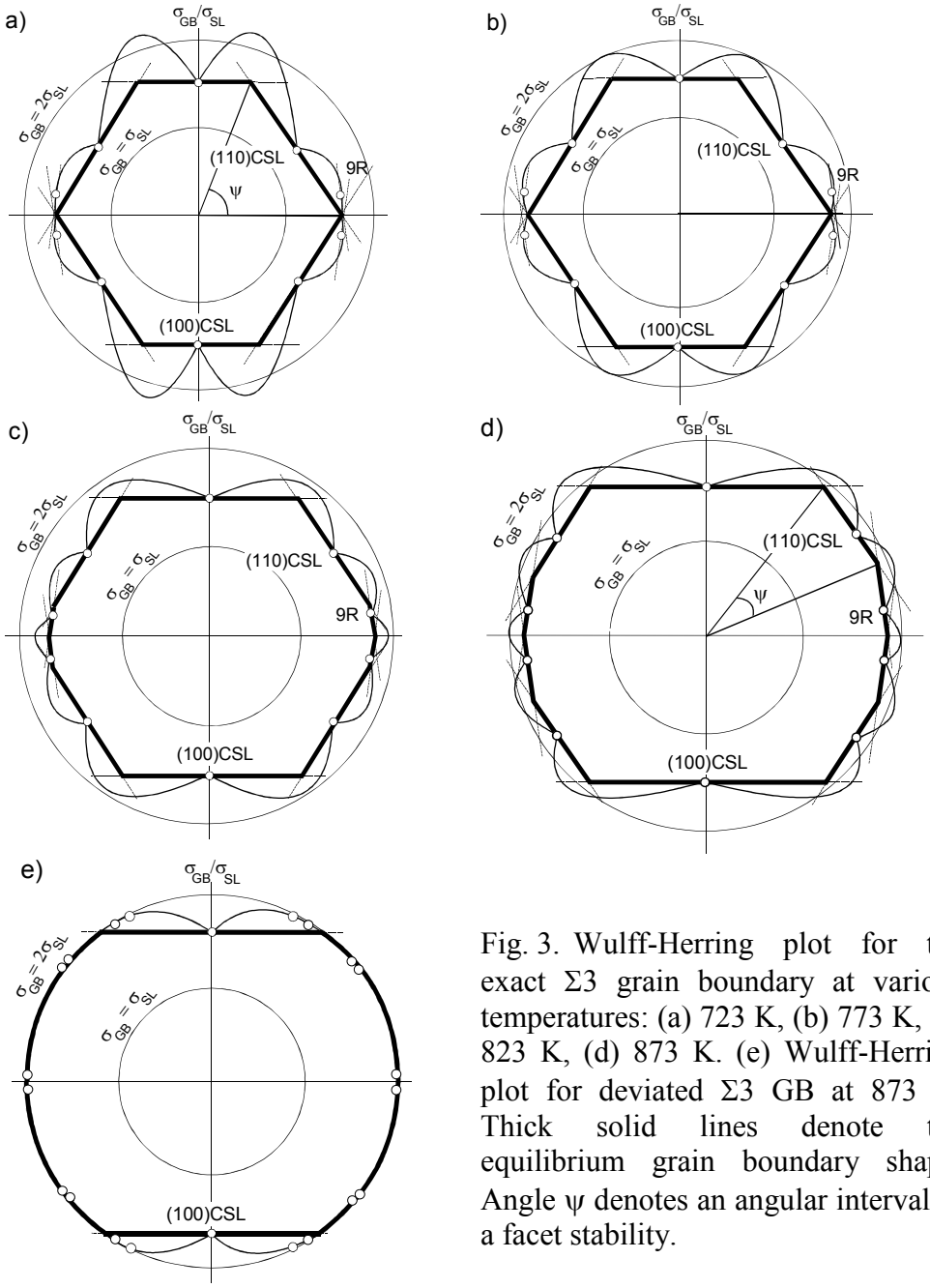

Fig. 3. Wulff-Herring plot for the exact Σ3 grain boundary at various temperatures: (a) 723 K, (b) 773 K, (c) 823 K, (d) 873 K. (e) Wulff-Herring plot for deviated Σ3 GB at 873 K. Thick solid lines denote the equilibrium grain boundary shape. Angle ψ denotes an angular interval of a facet stability.

Next closely packed CSL plane is $\{211\}_1/\{211\}_2$ [or $(010)_{\Sigma 3CSL}$] or so-called asymmetric twin. The angle between $(100)_{\Sigma 3CSL}$ and $(010)_{\Sigma 3CSL}$ facets is $\phi = 90°$. The presence of these facets is well documented for Al, Au, $AuCu_3$, and Ge [9–12]. The typical rectangular twin plates with $(100)_{\Sigma 3CSL}$ and $(010)_{\Sigma 3CSL}$ facets is observed, for example in Au thin films [10]. However, the twin plates in Cu and Ag are not rectangular. The end facet makes an angle of $\phi = 82°$ with the $\{111\}_1/\{111\}_2$ [or $(100)_{\Sigma 3CSL}$] sides [13]. TEM studies revealed that this $\phi = 82°$ facet has the so-called 9*R* structure forming a plate of bcc grain boundary phase in the fcc matrix [14–16]. The $(100)_{\Sigma 3CSL}$ and 82° 9*R* facets are clearly seen on the Σ3 twin plates also in our samples. Moreover, analysis of the available data shows that 82° 9*R* facet appears in Cu only at high temperatures [6]. At low temperatures the "normal" 90° $(010)_{\Sigma 3CSL}$ facets are present in Cu and coexist with 82° 9*R* facets [6]. In Al samples with the exact Σ3 the 82° 9*R* facet is present at high temperature, but the 90° $(010)_{\Sigma 3CSL}$ facet was not observed down to 0.77 T_m (Fig. 3). However, in the literature the 90° $(010)_{\Sigma 3CSL}$ facet was

observed in Al at 0.53 T_m [13]. With decreasing temperature the equilibrium length of a 82° 9*R* facet in Al as measured from the Wulff-Herring plots decreases almost down to zero (Figs. 3a to 3d). In deviated Σ3 Al GB the 82° 9*R* facet was absent at high temperature as well. It is significant that GB shape was stable at a very high temperature (close to the melting point) during long-term annealing of the samples. This fact together with obtained Wulff-Herring plots for 0.94 T_m allows us to suppose that close to T_m this is an equilibrium shape for GBs in investigated samples.

Let us compare the Wulff-Herring plots for Σ3 GBs in Al at 0.94 T_m (Fig. 3d) and Cu at 0.95 T_m [6]. In Cu the equilibrium shape of a Σ3 GB is a narrow plate. It is very similar to the typical twin plates, which are easy to observe in the microstructure of Cu and Cu alloys. The energy of symmetric twin in Cu is more that 10 times lower than that of a 82° 9*R* facet. This shape can be explained with a low stacking fault energy in Cu of 0.04-0.08 J/m^2 known from independent experiments [17–19]. Crystallographically, the stacking fault is nothing else as a symmetric twin GB $\{111\}_1/\{111\}_2$ or $(100)_{\Sigma 3CSL}$. The stacking fault energy in Al is 0.20-0.28 J/m^2 [20–24]. It is much higher than that of Cu. The energy of symmetric twin in Al is only slightly lower than that of a 82° 9*R* facet (Fig. 3d). Therefore, the twinning is not observed in Al and its alloys, and the equilibrium shape of a Σ3 GB in Al is not so flat as in Cu. The small $\Delta\theta = 0.8°$ deviation leads in Cu to the increase of σ_{GB} for the symmetric twin (as known from the literature, the structural intrinsic GB dislocations compensating the deviation $\Delta\theta$ appear in the near-coincidence GBs) [25]. In the same time, the energy of a 82° 9*R* facet remains almost unchanged. As a result the equilibrium shape of the Σ3 twin becomes broader with increasing $\Delta\theta$ than at exact coincidence, and the next closely packed facet becomes stable and appear in the equilibrium shape [25]. The 82° 9*R* facet appears instead of the 90° $(010)_{\Sigma 3CSL}$ facet at high temperature.

The $\phi = 56°$ facet with $\{100\}_1/\{122\}_2$ [or $(110)_{\Sigma 3CSL}$] was also observed for the exact Σ3 GB in Al [8]. This facet in the exact Σ3 boundary is present within a wider temperature range and remains stable even after a long annealing time in comparison with Cu [6]. However, the angular interval ψ, where this facet is stable becomes narrower with increasing temperature (Figs. 3 and 4). It can be supposed that near the melting point the facet $\{100\}_1/\{122\}_2$ [or $(110)_{\Sigma 3CSL}$] could disappear. In the low temperature range the facet $\{100\}_1/\{122\}_2$ becomes stable and has very low ratio σ_{GB}/σ_{SL} (Figs. 3 and 4). For deviated GB this facet is not detected. With increasing $\Delta\theta$ the formation of rounded rough grain boundary portions were observed. It can be supposed that with increasing $\Delta\theta$ the portion of faceted GB would decrease and that of rounded rough GB would increase. The facets will completely disappear at $\Delta\theta_c$ about 7-12° [26].

In Fig. 4 the phase diagram for Σ3 facets is shown according to the approach proposed in [5] for the equilibrium crystal shape. Instead of temperature the deviation from coincidence misorientation $\Delta\theta$ is plotted as an ordinate (Fig. 5). Filled circles correspond to the facets. Open squares relate to the rough GB portions. The stability field of the $(100)_{\Sigma 3CSL}$ facet exists both at exact coincidence and $\Delta\theta = 3°$. However, the stability field of the $(100)_{\Sigma 3CSL}$ facet becomes narrower with increasing $\Delta\tilde{\theta}$. The stability fields for $(110)_{\Sigma 3CSL}$ and 9*R* facets are restricted, exist only at low $\Delta\theta$ and do not extend to $\Delta\theta = 3°$. They transform into rounded rough GB portions. Therefore, starting from certain $\Delta\theta$ the equilibrium shape of Σ3 GB in Al becomes similar to that of grain boundary in Mo (metal with base-centred cubic lattice) [27]. This is the important difference of the equilibrium shape of Σ3 GB in Al (fcc metal with high stacking fault energy) and in Cu (fcc metal with low stacking fault energy).

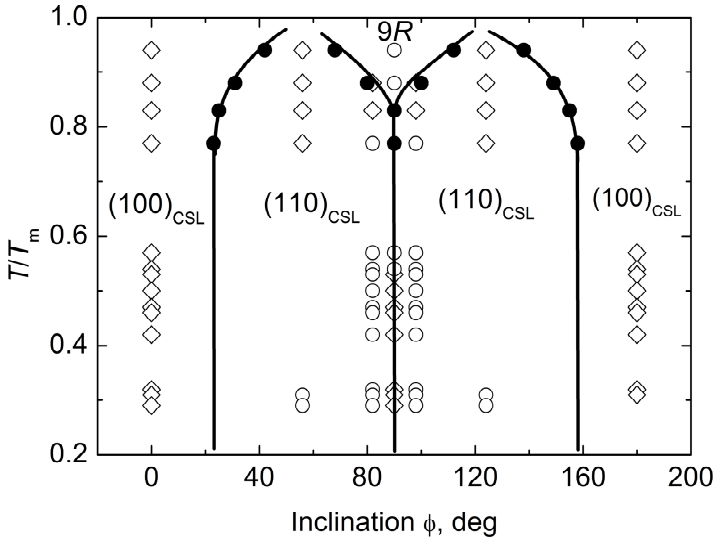

Fig. 4. Phase diagram for Σ3 facets in Al coordinates "Temperature"– "inclination ϕ" plots the angular regions for the faceted areas of GB shape. Full circles mark the borders between facets (obtained from Wulff-Herring plots, Fig. 3). Open circles mark temperatures where respective facets were not observed. Diamonds mark temperatures where respective facets were observed. Above 0.7 T_m are experimental data obtained in this work. Below 0.7 T_m are experimental data taken from [12–15]. Only CSL indexes are given in the figure, the respective lattice indexes are: $\{111\}_1/\{111\}_2$ for $(100)_{\Sigma 3CSL}$, $\{211\}_1/\{211\}_2$ for $(010)_{\Sigma 3CSL}$, $\{100\}_1/\{112\}_2$ for $(110)_{\Sigma 3CSL}$.

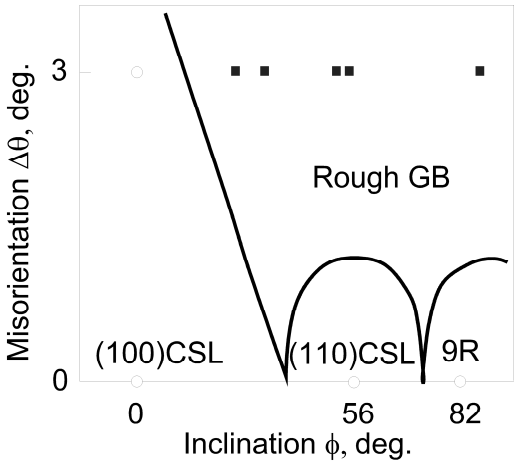

Fig. 5. Phase diagram for Σ3 facets in Al according to the approach [5] for the equilibrium crystal shape in coordinates "deviation from coincidence misorientation Δθ"– "inclination ϕ". Open circles correspond to the facets. Filled squares relate to the rough grain boundary portions

Conclusions

1. The exact Σ3 <110> tilt grain boundary and grain boundary deviated on Δθ = 3º from the exact Σ3, in semi-cylindrical Al bicrystals presenting all crystallographically possible inclinations with respect to the <110> tilt axis, become faceted upon annealing between 0.77 and 0.94 T_m.
2. The $\{111\}_1/\{111\}_2$ or $(100)_{\Sigma 3CSL}$, $\{100\}_1/\{112\}_2$ or $(110)_{\Sigma 3CSL}$, facets and the non-CSL 82°9*R* facet are observed for the exact Σ3 GB. These facets form sharp edges.
3. Only $\{111\}_1/\{111\}_2$ or $(100)_{\Sigma 3CSL}$ facet is observed for the deviated Σ3 GB with Δθ = 3º. Other where the deviated GB is rounded.
4. Wulff-Herring plots, constructed on the basis of GB energy measurements for the various facets (relatively to the surface energy; on the basis of liquid phase groove profile measurement) allowed determination of the equilibrium crystal shape (ECS) as a function of temperature
5. For the exact Σ3 grain boundary of the $(100)_{\Sigma 3CSL}$, $(110)_{\Sigma 3CSL}$, and non-CSL 9*R* facets are stable. Upon increasing Δθ $(110)_{\Sigma 3CSL}$, and non-CSL 9*R* facets disappear from the equilibrium shape of Σ3 grain boundary, i.e. roughening temperature for $(110)_{\Sigma 3CSL}$ and 9*R* facets is higher than T_m for the exact Σ3 grain boundary and lower than T_m for deviated grain boundary

Acknowledgements

This work was supported by the Russian Foundation of Basic Research (contract 05-02-16528), INTAS (contract 05-109-4951), German Federal Ministry for Education and Research (contract RUS 04/014).

References

[1] J.M. Paik, Y.J. Park , M.S. Yoon, J.H. Lee, Y.C. Joo: Scripta mater Vol. 48 (2003), p. 683
[2] J.S. Choi, D.Y. Yoon: ISIJ International Vol. 41 (2001), p. 478
[3] J.B. Koo, D.Y. Yoon: Metall. Mater. Trans. A Vol. 32 (2001), p. 469
[4] M. Yoon, S.G.J. Mochrie, M.V. Tate, S.M. Gruner, E.F. Eikenberry: Surf. Sci. Vol. 411 (1998), p. 70
[5] C. Rottman, M. Wortis: Phys. Rev. B Vol. 24 (1981);:6274 and Vol. 29 (1984), p. 328
[6] B.B. Straumal, S.A. Polyakov, E.J. Mittemeijer: Acta Mater. Vol. 54 (2006), p. 167
[7] O. Kogtenkova, B. Straumal, S. Protasova, S. Tsurekawa, T. Watanabe: Zt. Metallkd. Vol. 96 (2005), p. 216
[8] O.A. Kogtenkova, B.B. Straumal, S.G. Protasova, P. Zięba: Def. Diff. Forum Vols. 237–240 (2005), p. 603
[9] J.M. Pénisson, U. Dahmen, M.J. Mills: Phil. Mag. Lett. Vol. 64 (1991), p. 277
[10] P.J. Goodhew, T.Y. Tan, R.W. Balluffi: Acta metall. Vol. 26 (1978), p. 557
[11] F.D. Tichelaar, F.W. Schapink: J. Phys. Paris C5 Vol. 49 (1988), p. 293
[12] A. Bourret, J.J. Bacmann: Inst. Phys. Conf. Series Vol. 78 (1985), p. 337
[13] A. Barg, E. Rabkin, W. Gust: Acta metall. mater. Vol. 43 (1995), p. 4067
[14] U. Wolf, F. Ernst, T. Muschik, M.W. Finnis, H.F. Fischmeister: Phil. Mag. A Vol. 66 (1992), p. 991
[15] F. Ernst, M.W. Finnis, D. Hoffmann, T. Muschik, U. Schönberger, U. Wolf: Phys. Rev. Lett. Vol. 69 (1992), p. 620
[16] D. Hofmann, M.W. Finnis: Acta metall. mater. Vol. 42 (1994), p. 3555
[17] N.I. Noskova, V.A. Pavlov, S.A. Nemnonov: Fiz. Metall. Metallogr. Vol. 20 (1965), p. 920
[18] L. Vassamillet, T. Massalski: J. Appl. Phys. Vol. 34 (1963), p. 3398
[19] G. Carlos: Trans AIME Vol. 233 (1965), p. 1965
[20] V.A. Finkel, V.I. Papirov: Fiz. Metall. Metallogr. Vol. 26 (1968), p. 1108
[21] J. Edington, D. Smallman: Phil. Mag. Vol. 11 (1965), p. 1109
[22] I. Dillamore, R. Smallman: Phil. Mag. Vol. 12 (1965), p. 191
[23] E. Aerts, P. Delavignette, C. Siems: J. Appl. Phys. Vol. 33 (1962), p. 3078
[24] H. Seeman, K. Scharr: Phys. Stat. Sol. Vol. 4 (1964), p. 89
[25] B. Straumal, S. Polyakov, E. Bischoff, E. Mittemeijer: Zt. Metallkd. Vol. 95 (2004), p. 939
[26] Straumal BB, Shvindlerman LS. Acta metall 1985;33:1735.
[27] B.B. Straumal, V.N. Semenov, O.A. Kogtenkova, T. Watanabe: Phys. Rev. Lett. Vol. 192 (2004), p. 196101